Informatics in Medicine Unlocked 33 (2022) 101069

Contents lists available at ScienceDirect

Informatics in Medicine Unlocked

journal homepage: www.elsevier.com/locate/imu

Computational modeling of potential milciclib derivatives inhibitor-CDK2 binding through global docking and accelerated molecular dynamics simulations

Mushira Khanam [b,1], Abu Tayab Moin [a,1], Kazi Ahsan Ahmed [c], Rajesh B. Patil [e], Abul Bashar Ripon Khalipha [f], Nafisa Ahmed [d], Rajat Bagchi [f], Md Asad Ullah [g], Jannatul Ferdoush [h], Saiful Islam [i], Bashudev Rudra [a,*]

[a] Department of Genetic Engineering and Biotechnology, Faculty of Biological Sciences, University of Chittagong, Chattogram, Bangladesh
[b] Department of Biochemistry and Molecular Biology, Life Science Faculty, Bangabandhu Sheikh Mujibur Rahman Science and Technology University, Gopalganj, Bangladesh
[c] Department of Biochemistry and Molecular Biology, Faculty of Agriculture, Bangladesh Agricultural University, Mymensingh, Bangladesh
[d] Biotechnology Program, Department of Mathematics and Natural Sciences, School of Data and Sciences, BRAC University, Dhaka, Bangladesh
[e] Department of Pharmaceutical Chemistry, Sinhgad Technical Education Society's, Sinhgad College of Pharmacy, Vadgaon (Bk), Maharashtra, India
[f] Department of Pharmacy, Life Science Faculty, Bangabandhu Sheikh Mujibur Rahman Science and Technology University, Gopalganj, Bangladesh
[g] Department of Biotechnology and Genetic Engineering, Faculty of Biological Sciences, Jahangirnagar University, Savar, Dhaka, Bangladesh
[h] Department of Pharmacology, BGC Trust Medical College, Chattogram, Bangladesh
[i] Bangladesh Council of Scientific and Industrial Research (BCSIR), Chattogram Laboratories, Chattogram, Bangladesh

ARTICLE INFO

Keywords:
Hepatocellular carcinoma
Milciclib
Anticancer drug
Halogenated derivatives
Molecular docking
Non-bond interactions
Molecular dynamics simulation

ABSTRACT

Hepatocellular carcinoma (HCC) is the most common malignant condition of the liver that occurs as a result of uncontrolled cellular proliferation after a series of disruptions at cell cycle regulatory checkpoints in the normal cell. Due to the lack of appropriate therapeutics or remedial treatment methods, new treatment strategies against HCC need to be developed. Cyclin dependent kinases (CDKs) are required to control the cell cycle and apoptosis, but their overexpressionis critical in the progression of cancer and is often expressed in HCC. Thus, CDKs are considered a promising class of target-defined therapy for HCC. Milciclib is a potential candidate for HCC which exhibits inhibitory activity against CDK2 leading to cell cycle arrest and apoptosis of tumor cells. Herein, we have halogenated the parent drug milciclib to improve its efficacy against CDK2. The primary structure of milciclib (D) was modified with F, Cl and,CF_3 groups. The frontier molecular orbital features, binding affinity, non-bonded interaction and the pharmacokinetic parameters were analyzed for milciclib and its derivatives. We also performed molecular docking and extended molecular dynamics simulation studies to study the binding interactions and binding affinity more closely. Our computational investigation showed the derivatives D-F and D-CF_3 have significant chemical reactivity, the best binding affinity, nonbonding interactions, and improved pharmacokinetic properties compared to the parent drug milciclib. Molecular dynamics analysis and MM-PBSA calculations indicated that D-Cl had a slightly more stable conformation and higher binding affinity compared to D-CF_3.

1. Introduction

Hepatocellular carcinoma (HCC), the most prevalent form of liver cancer, accounts for 90% of primary liver cancer and has grown to become the fourth leading cause of cancer-related mortality worldwide. The progression of HCC in patients is driven by underlying cirrhosis and chronic liver inflammation [1]. Chronic liver disease caused by hepatitis B virus infection is the most common cause of HCC worldwide, followed by hepatitis C infection and other risk factors such as high alcohol consumption, tobacco smoking, nonalcoholic fatty liver disease and insulin resistance [1,2]. Current therapy for HCC comprises of surgical resection, Orthotropic liver transplantation (OLT), percutaneous

* Corresponding author.
E-mail address: bashudev@cu.ac.bd (B. Rudra).
[1] These authors contributed equally to this work.

https://doi.org/10.1016/j.imu.2022.101069
Received 16 February 2022; Received in revised form 21 August 2022; Accepted 26 August 2022
Available online 31 August 2022

ethanol injection, radiofrequency ablation, *trans*-arterial chemoembolization and radio embolization, among which OLT is considered the best therapeutic option for both HCC and underlying cirrhosis [3]. However, HCC is asymptomatic in early stages and the majority of patients are diagnosed only at advanced stages of HCC [1,4]. Unfortunately, patients with late-stage HCC are not eligible for curative surgeries such as OLT and have limited therapeutic options [3]. The lack of accessible and efficient therapeutical or remedial treatment methods has prompted the development of novel treatment strategies. Meanwhile, it is necessary to modify currently approved drugs such as milciclib in order to improve their efficacy, as well as to develop new and more effective HCC therapies [5].

The mammalian cell cycle consists of five distinct stages- Gap 0 phase (G_0), in which the cells are in a resting state, Mitosis phase (M) during which the cell divides into two daughter cells, Synthesis phase (S) during which the cell replicates its genetic material and the Gap phases 1 and 2 (G1 and G2) separating M and S phase during which cell growth and RNA and protein synthesis occur [6]. Each of the five distinct phases of the cell cycle are controlled by specific Cyclin dependent kinases complexes (CDK/Cyclin complexes) composed of CDKs and their binding partners, cyclin regulatory subunit [6,7].CDKs are members of the serine/threonine kinase family that when complexed with cyclins, regulate cell cycle progression, RNA transcription, and apoptosis, making them promising targets for anticancer drug development [7,8]. Oncogenic alterations of CDKs have been found to be associated with human cancers. Upregulation of CDKs leads to loss of cell cycle checkpoint integrity, resulting in unregulated cell regeneration and rogue hepatocyte proliferation, all of which contribute to the development of HCC [4]. Moreover, the inhibition of CDKs has been demonstrated to promote apoptosis in cancer cells, making CDK inhibition particularly appealing from the perspective of cancer therapy [7,9]. Cyclin-dependent kinase 2 (CDK2) is active during the G1/S and M phases of the cell cycle and is essential for cell centrosome replication [10]. It ensures that the centrosome replicates only once. The kinase activity of CDK2 is highly elevated in many cancers including HCC [4]. CDK2 is the major enzymatic modifier of the p53, the tumor suppressor whose functional loss is a critical factor in HCC development [4]. Dysregulated CDK2 complex induces aberrant cell proliferation in HCC and downregulation of CDK2 in HCC cell lines results in cancer cell arrest [4]. Therefore, CDK2 is an attractive therapeutic target for HCC. In this study, we have used PubChem compound database to collect the protein crystal structure of CDK2- 6Q4, 6Q4E, 6Q4G, 6Q4H, 6Q4J, 6Q48, and 6Q49 to use as the target protein.

Owing to the absence of proper preventive or curative treatment methods against HCC, there is an urgent need for new therapeutic strategies. A potent CKD2 inhibitory drug called milciclib (PHA-848125) has been developed by Tiziana Life Sciences [10]. Belonging to the pyrazolo (4,3-h) quinazoline chemical class, this drug blocks the G1 phase of the cell cycle and inhibits CDK2, leading to cell cycle arrest [10]. Moreover, milciclib has exhibited the reduction of miR-221 and miR-222 expression *in vivo* resulting in an elevated amount of tumor suppressors CDKN1B/p27kip and CDKN1C/p57kip [5,11]. Tumor suppressor genes, p27 and p57, inhibit the overexpression of CDK2, causing the tumor cell to undergo cell cycle arrest and apoptosis. Inhibitory activity of Milciclib (PHA-848125AC) is not exclusive to only CDK2 but is also effective against closely related CDKs such as CDK1, CDK4, CDK5 and CDK7 [5,12]. Inhibition of these kinases may cause cell cycle arrest and apoptosis in tumor cells. Milciclib has been shown to be effective in preclinical investigations against brain tumors such as medulloblastoma and glioma, as well as non-small cell lung cancer in a transgenic mice model [13]. Milciclib has also proven efficacy in xenograft models against melanoma, ovarian, colon, pancreatic, prostate, and non-small cell lung cancer, inhibiting tumor development by 64–91% [13]. Milciclib in phase I clinical trials has proven to bring improvement in patients with advanced solid tumors of the colon, thymus, and pancreas [10,13]. It is being tested in in phase II clinical trials as an oral anticancer therapy for patients with advanced HCC [10,13]. Hence, milciclib is a promising candidate for the treatment of patients with HCC.

Halogen bonding creates highly directed stabilizing contact between the halogenated ligands and their protein substrate, increasing binding affinity between the ligand and the protein [14–16]. Since halogen bonding enhances strong interactions between halogenated ligands and their target proteins, halogenation of existing inhibitors, in this case milciclib, is a promising way to improve the efficacy of the drug [17,18]. Moreover, halogen bonding extends the drug's lifetime and fills the hydrophobic spaces in the protein binding site, allowing the drug molecule to pass through biological barriers more easily, enhancing oral absorption and permitting blood–brain barrier crossing [19]. The ease of absorption and longer lifetime are particularly useful because inhibitors should be well absorbed and retained by cancer cells for a sufficient period so that the drugs can wield a desired pharmacological effect. In fact, the use of fluorinated derivatives of existing drugs to improve their efficacy has made significant contributions in medicinal chemistry and drug design, and it is now becoming increasingly popular [20–23].

In the present work, the structure of the parent drug milciclib (D) was modified with F, Cl, CF_3, groups. The modified derivatives were then optimized to examine their biochemical behavior based on the quantum mechanical approach. Thereafter, we calculated the HOMO-LUMO gap, hardness and softness of milciclib, and its halogenated derivatives. To better understand the binding affinity, mode, and interaction between the drugs and the amino acid residues of CDK2, we implemented molecular docking and nonbonding analysis. The derivatives D-F and D-CF_3 of milciclib (D) were found to have significant chemical reactivity, binding affinity, nonbonding interactions, and improved pharmacokinetic properties compared to the parent drug. Thus, new experimental milciclib derivatives, D-F and D-CF_3, may play a central role in the treatment of HCC.

2. Materials and computational methods

2.1. Preparation and optimization of ligands

Initial three-dimensional structure of milciclib was retrieved from PubChem (https://pubchem.ncbi.nlm.nih.gov/), an open access chemistry database maintained by the National Center for Biotechnology Information (NCBI). This rapidly growing public repository allows researchers to explore the properties of a specific bioactive molecule, or a drug candidate, or even a known drug on a wider scale in order to find potentially novel functions or off-target effects [24].The structure of the parent drug, milciclib (D), was modified by substituting the –CH3 group at its 9 N position with F, Cl, -CF_3 functional groups to obtain new milciclib derivatives: D-F, D-Cl, D-CF_3respectively. For achieving the optimum conformational structure, molecular geometry optimization of milciclib and the newly generated milciclib derivatives was performed in Chem3D Pro 12.0 software (software CS Chem3D Pro® version 12.0). ^{1}H NMR prediction of the ligands is required to determine their stability and stoichiometry [25,26]. Therefore, ChemDraw Ultra software (software CS ChemBioDraw® Ultra, version 11.0.1) was utilized to generate the ^{1}H NMR estimation. ^{1}H NMR prediction of milciclib and the derivatives showed that all ligands are stable (Fig. 1).

2.2. Preparation of target protein for molecular docking

The milciclib ligands were subjected to a molecular docking study against the target protein, cyclin-dependent kinase 2 (CDK2). Crystal structures of CDK2, namely 6Q4D, 6Q4E, 6Q4G, 6Q4H, 6Q4J, 6Q48, and 6Q49, were obtained from RCSB Protein Data Bank (PDB) database (https://www.rcsb.org/). The RCSB PDB database allows users to view and visualize 3D shapes of proteins, nucleic acids, and complex assemblies by using curated 3D macromolecular data from the PDB archive [27].Energy minimization of all the crystal structures was conducted

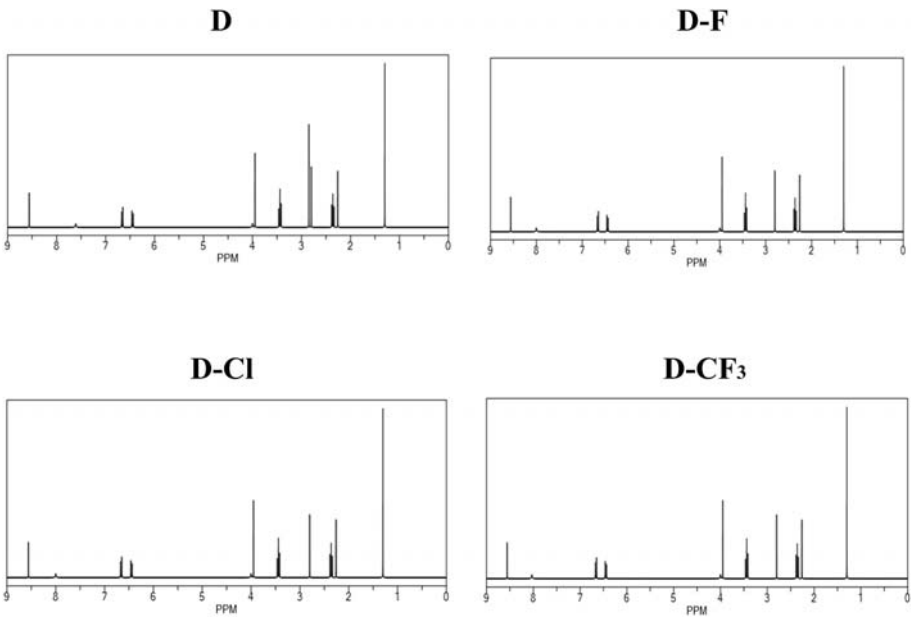

Fig. 1. Chem3D Pro 12.0 ^{1}H NMR spectrum estimation of the ligands: D, D-F, D-Cl, D-CF_3. The shift calculation for protons of the ligands are shown in the figure. The numbers represent the predicted shift of the signals in ppm.

with Swiss-PDBViewer v4.1.0 (https://spdbv.vital-it.ch/) to find the optimum structural arrangement of amino acid residues. Prior to docking, all the heteroatoms, water molecules, and multiple chains were removed from the crystal structures using PyMOL (The PyMOL Molecular Graphics System, Version 1.7.4.5 Schrödinger,LLC) Software packages. PyMOL is a free cross-platform molecular graphics system that enables conformational editing, rudimentary chemical editing and molecular editing at various levels, allowing users to design new objects by removing atoms from existing object or by merging them [28].

2.3. Molecular docking and non-bonded interaction analysis

Molecular docking is a powerful tool in computational drug design that can predict the binding modes of a ligand with a target protein having a known three-dimensional structure [29]. For examining the optimal orientations of the ligands and the target proteins which yielded the maximum binding affinity, molecular docking was performed using AutoDock Vina in the PyRx platform (https://pyrx.sourceforge.io/). AutoDock Vina is a relatively molecular docking program that uses a sophisticated gradient optimization method to achieve faster execution and more accurate binding mode prediction compared AutoDock 4 [30]. Afterwards, BIOVIA Discovery studio visualizer v16.1.0.15350 (version 16.1.0.15350, Biovia, USA)was employed to visualize the interaction and binding of the ligands and the target proteins. For the generated protein-ligand complexes, various non-bonded interactions such as hydrogen bond interaction and hydrophobic bond interaction with specific distance were also visualized using the Discovery Studio visualizer in order to select complexes with the best binding affinity.

2.4. Study of pharmacokinetic parameters

The pharmacokinetic parameters of milciclib and its modified derivatives, such as drug absorption, metabolism, toxicity, and carcinogenicity were analyzed using the admetSAR online database and Medchem Designer software (http://simplus-downloads.com/). AdmetSAR is an open source, comprehensive computer readable database that collects available ADMET-associated properties (absorption, distribution, metabolism, excretion, and toxicity) data from the published literature and predicts ADMET-associated properties of a variety of molecules [31]. The toxicity of the drugs were also evaluated using the PreADMET server (https://preadmet.bmdrc.kr/). PreADMET is also a web-based application that can perform molecular descriptors calculation, drug likeness prediction, ADME prediction as well as toxicity prediction [32]. Throughout the entire generation process, structure data file (SDF) and simplified molecular-input line-energy system (SMILES) strings of the modified derivatives were used.

2.5. Molecular dynamics simulation studies and MM-PBSA calculations

To gain deeper insights of binding interactions and binding affinity in a simulated biological environment, molecular dynamics simulations (MDS) and MM-PBSA calculations were performed on the docked complexes comprised of the most promising ligands, D-CF_3 and D-F, and the target protein 6Q4H. Gromacs 2020.4 MDS program was employed to perform 200 ns production phase MDS of respective equilibrated systems [33].To complete the computationally intensive MDS tasks, the HPC cluster at Bioinformatics Resources and Applications Facility (BRAF), C-DAC, Pune was utilized. The crystal structure of CDK2 with co-crystallized halogenated compound as a ligand (PDB ID: 6Q4H) is available with reasonably good resolution (1.0 Å) in the RCSB protein databank. However, in this crystal structure the terminal residues 1–7, and the residues 39–44 and 154–155 are reported as missing residues. Though these residues does not belong to the binding site, as a prerequisite of MDS studies, these non-terminal residues were modeled by fill missing residues utility of Modeller 9.12 program [34] in Chimera interface. The topology of the protein was prepared using CHARMM-36 force field parameters [35,36], while the topologies of the ligand were generated from CGenFF server with CHARMM General Force Field [36, 37]. The system was solvated with the default simple point charge water model (SPC216) in a dodecahedron unit cell [38]. The resulting solvated systems were neutralized with the addition of four chloride ions respectively. In order to remove the steric clashes, the unrestrained energy minimization was performed with the steepest descent criteria. The resulting system was equilibrated at constant volume and temperature setting of 300 K using modified Berendsen thermostat [39], and then at a constant volume and pressure Berendsen barostat [40] for 1 ns each. The equilibrated systems were the subjected to the production phase MDS of 100 ns where all the covalent bonds were restrained with the LINCS algorithm [41]. The long-range electrostatic interaction energies (Coulomb and Lennard Jones interaction energies) were

measured with the cut-off of 12 Å with the Particle Mesh Ewald method (PME) [42]. During the production phase MDS, the modified Berendsen thermostat and Parrinello-Rahman barostat [43] were used for temperature and pressure coupling respectively. The MDS trajectories were analyzed to measure root mean square deviations (RMSD) in backbone atoms and ligand atoms, root mean square fluctuations (RMSF) in the side chain atoms of each residue, radius of gyration (Rg) from the center of mass of protein, and number of hydrogen bonds formed between ligand atoms and residues at bindings site. The MD trajectories starting from 150 ns to 200 ns isolated at each 100 ps were used to calculate the binding free energies of ligands with the Poisson Boltzmann surface area continuum solvation (MM-PBSA) calculations [44,45]. Further, per residue domain decomposition analysis was performed to identify the key residues contributing in binding free energy.

3. Results and discussion

^{1}H NMR prediction of milciclib and the derivatives D-CF_3, D-Cl, and D-F, are shown in Fig. 1. The frontier molecular orbitals of milciclib (D), and its modified derivatives are presented in Supplementary Fig. S1. The binding and interaction of D, D-F, D-Cl, D-CF_3 with protein 6Q4H are shown in Fig. 2. The non-bond interaction of D and its derivatives with protein 6Q4H as are presented in Supplementary Fig. S2. The hydrophobic binding sites of the potential drugs when docked against protein 6Q4H are exhibited in Supplementary Fig. S3. Hydrogen bond surface of 6Q4H with D, D-F, D-Cl, D-CF_3 is shown in Fig. 3. The superimposed structures of pre- and post-MD states of D-CF_3-6Q4H, D-Cl-6Q4H, D-F-6Q4H, and D-6Q4H complexes are shown in Fig. 4. The MD trajectory snapshots for both complexes at various time intervals are shown in Fig. 5. The RMSD in protein backbone atoms and the RMSD in ligand atoms for D-CF_3, D-Cl, D-F, and milciclib complexes are displayed in Fig. 6. The protein-ligand interactions captured from the initial and post-MD poses of all four ligands at the binding pocket of 6Q4H are shown in Fig. 7. The results of RMSF measurement of the protein-ligand complex are shown in Fig. 8A. The Radius of gyration of Cα atoms of 6Q4H bound with each ligand are shown in Fig. 8B. The number of hydrogen bonds formed between the ligands and binding site residues are shown in Fig. 8C. The results of hydrogen bond % occupancy evaluation of both ligands, D-CF_3, D-Cl, D-F and milciclib are displayed in Supplementary Fig. S4. The results of MM-PBSA calculation are shown in Fig. 9A, while the results of per residue energy decomposition analysis are shown in Fig. 9B.

The HOMO-LUMO energies gap, hardness, and softness of milciclib (D) and its derivatives D-F, D-Cl, D-CF_3 are presented in Supplementary Table S1. The binding energy of Milciclib and the modified derivatives against the target proteins (6Q4D, 6Q4E, 6Q4G, 6Q4H, 6Q4J, 6Q48, and 6Q49) are shown in Supplementary Table S2. The binding affinity and non-bond interactions of milciclib (D) and its derivatives D-F, D-CF_3 and D-Cl with 6Q4H are shown in Table 1. AdmetSAR values for milciclib (D) and its derivatives are given in Table 2. The ADMET values calculated by MedChem Designer Software of milciclib and its derivatives are shown in Supplementary Table S3. The result of toxicity analysis of milciclib and its derivatives (D-F, D-CF_3, D-Cl) conducted by preADMET are presented in Supplementary Table S4. The average, minimum and maximum values of the MDS analysis for D-CF_3-6Q4H, D-Cl-6Q4H, D-F-6Q4H, and D-6Q4H complexes are shown in Table 3. The results of MM-PBSA calculations for both ligands are listed in Table 4.

3.1. Hardness and softness analysis of potential drugs by calculating HOMO and LUMO energy level

The frontier molecular orbital features, the highest occupied molecular orbitals (HOMOs) and lowest unoccupied molecular orbitals (LUMOs), play critical roles in chemical reactions [46]. The HOMO-LUMO energy gap is associated with the chemical hardness, softness, the kinetic stability, and the chemical reactivity of a drug

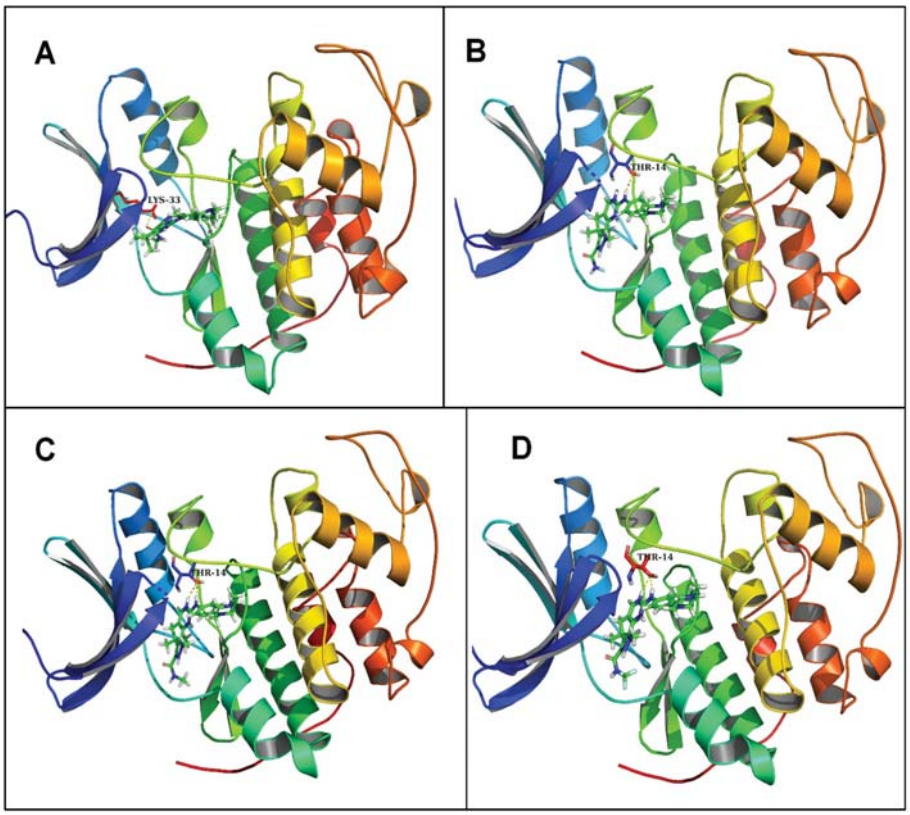

Fig. 2. Molecular docking analyses showing (A) the binding of milciclib- D, (B) derivative D-F, (C) derivative D-Cl, and (D) derivative D-CF_3 with protein 6Q4H.

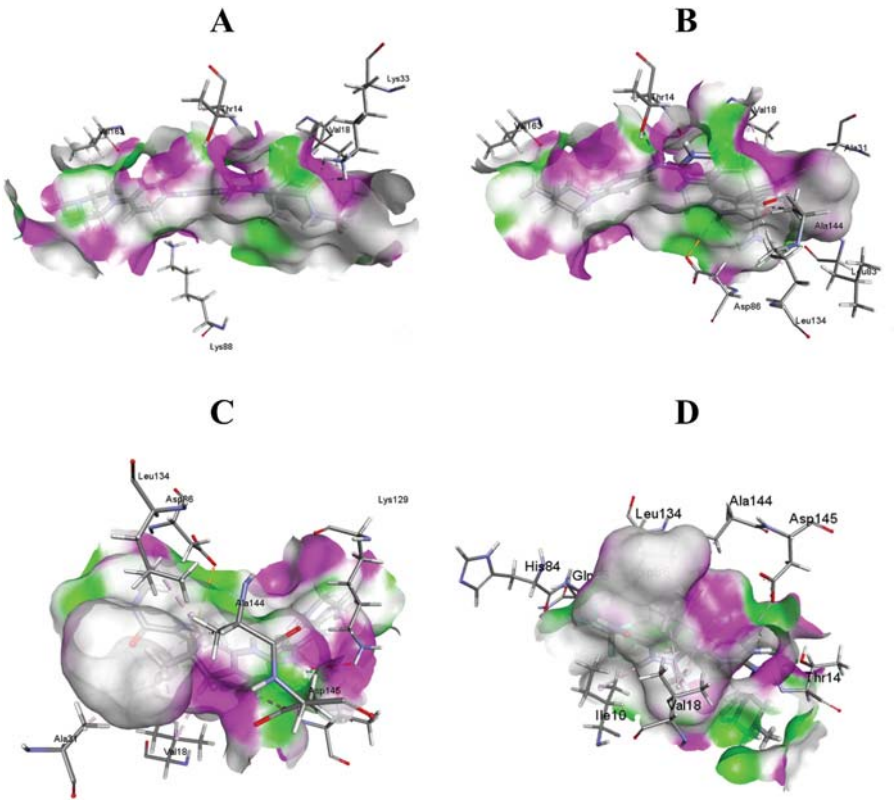

Fig. 3. Hydrogen bond surface of (A) milciclib- D, (B) derivative D-F, (C) derivative D-Cl, and (D) derivative D-CF3 with protein 6Q4H. The hydrogen donor is represented by the pink regions, while the hydrogen acceptor is represented by the lime areas. The amino acid THR14 (2.25 and 2.21) formed two strong hydrogen bonds with the derivative D-CF3. (For interpretation of the references to color in this figure legend, the reader is referred to the Web version of this article.)

molecule. A smaller energy gap and increased softness indicate that the drug molecule has higher polarity and chemical reactivity whereas a large energy gap indicates high kinetic stability and low chemical reactivity [47,48]. The parent drug milciclib (D) was found to have the lowest energy gap values, the lowest hardness value, and the highest softness value. Among its modified derivatives, D-CF_3 exhibited the lowest energy gap values, the lowest hardness value and the highest softness value. Supplementary Table S1 lists the HOMO and LUMO energy values, the energy gap, hardness, and softness of all drug candidates. The following equations were utilized to calculate HOMO-LUMO, gap, hardness (η), and softness (S) values of the drugs [49].

$$\eta = [\varepsilon LUMO - \varepsilon HOMO]/2$$

$$S = 1/\eta$$

3.2. Interaction and binding affinity of the potential drugs with the target proteins

The docking score determines the extent of molecular interaction between the ligands and the active site of the target receptor [50]. The more negative the binding energy, the more favored the orientation and the more stable the conformation of the ligand-receptor complex will be. The docking scores of milciclib and its derivatives against proteins 6Q4D, 6Q4E, 6Q4G, 6Q4H, 6Q4J, 6Q48, 6Q49 are shown in Supplementary Table S2. When compared to the parent drug milciclib (D), which had a binding energy of −9.5 kcal/mol with protein 6Q4H, the derivatives D-F and D-C F_3 had a better binding affinity of −10.3 kcal/mol with the same protein. Since milciclib and its derivatives had the maximum binding energy with protein 6Q4H, we selected 6Q4H protein as our potential target for our further studies. The binding interaction of milciclib (D) and derivatives D-F, D-Cl, D-CF_3 with protein 6Q4H are shown in Fig. 2.

Trifluoromethyl (-CF_3) group has been broadly used in drug design due to its strong electronegativity, lipophilic nature as well as its physiochemical, biological, and pharmacokinetic properties [51].Fluorination, in particular,is popular in medicinal chemistry and drug designbecause of its significant impact on drug potency, permeability, metabolism, and pharmacokinetic properties [52].When the potential drugs were docked against 6Q4H, the D-CF3-6Q4H complex showed improved hydrogen bonding compared to the parent drug (D). Despite the fact that hydrogen bonding has a less impact on the free binding energy, it results in higher binding affinity and greater binding specificity [53,54].The derivative D-CF_3 also possessed other non-bond interactions such as hydrophobic bond, halogen bond and electrostatic bond during their binding (Table 1). The hydrophobic surface and hydrogen bond surface of milciclib (D) and derivatives with 6Q4H protein are shown in Supplementary Fig. S3 and Fig. 3, respectively.

Hydrogen bonds determine the preciseness of ligand binding and therefore, have play an important role in drug binding [55,56]. The structures and reactivity of numerous molecular processes are also regulated by intermolecular hydrogen bonding [57,58]. According to a study conducted by Wade et al., hydrogen bonds of <2.3 Å can enhance binding affinity by several orders of magnitudes. When docked against 6Q4H, hydrogen bonding with THR14 residue is observed in milciclib (D) and its derivatives D-F, D-Cl and D-CF_3. The derivative D-CF_3 exhibited two strong hydrogen bonds with amino acid THR14 (2.25 Å and 2.21 Å), whereas the primary drug milciclib did not exhibit any strong hydrogen bonding with 6Q4H. The D-F-6Q4H complex showed no strong hydrogen bonding but the D-Cl-6Q4H complex exhibited a strong hydrogen bonding with amino acid THR14 (2.15 Å).

In our study, the D-CF_3-6Q4H complex exhibited three halogen bonds with HIS84 (3.31 Å), GLN85 (3.46 Å), and ASP86 (3.18 Å) amino acid residues (Table 1). Lu et al. study suggested that halogen bonding increased the stability of a protein-ligand receptor and also contributed

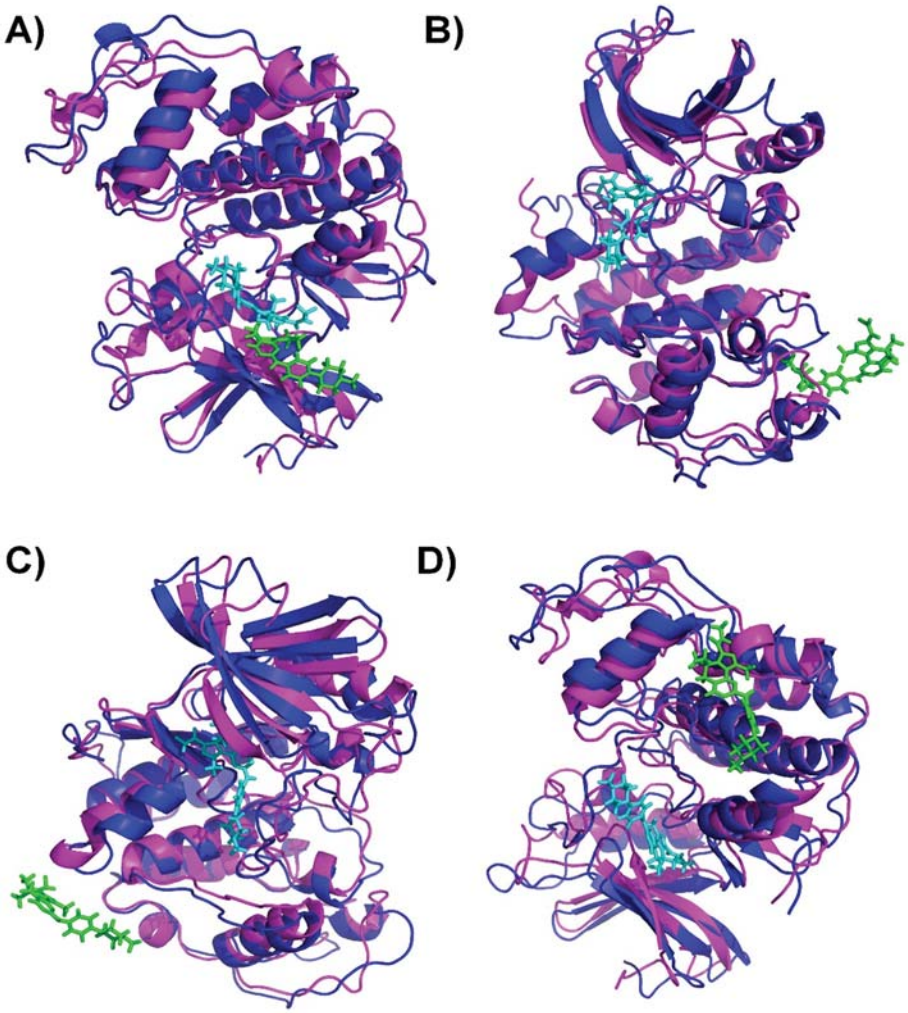

Fig. 4. The superimposed structures of pre-MD state (protein in magenta and ligands in cyan color) and post-MD state (protein in blue and ligands in green color) of complexes. A) Complex of 6Q4H with bound D-CF_3, B) Complex of 6Q4H with bound D-Cl, C) Complex of 6Q4H with bound D-F, and D) Complex of 6Q4H with bound milciclib. (For interpretation of the references to color in this figure legend, the reader is referred to the Web version of this article.)

to binding affinity selectivity [59]. Among the modified drugs, D-$CF_3$was found to have the highest softness, which may enhance the drug's polarizability and simulate more nonbonding interactions with the receptor.

Pi-alkyl interactions in biological systems represent a strong and stable perpendicular (edge-to-face) orientation, which may contribute to higher ligand-protein binding affinity [60]. In our study, D-CF_3 showed five hydrophobic bonds with 6Q4H, one of which was a pi-alkyl bond formed by the amino acid ILE10 (5.35 Å) (Table 1). Two pi-alkyl bonds are observed in D-F with amino acid residues VAL18 (5.48 Å) and ILE10 (5.20 Å), and one pi-alkyl bond is observed in D-Cl with amino acid ILE10 (5.45 Å). However, the parent drug milciclib (D) only formed alkyl bonds with amino acids ILE10 (5.18 Å and 4.20 Å), VAL18(3.64 Å) and VAL163(4.74 Å).Electrostatic bond interaction with ASP86 residue was also observed in D-CF_3-6Q4H, D-F-6Q4H and D-Cl-6Q4H complexes.

3.3. Pharmacokinetic activity analysis of the compounds

The AdmetSAR values for milciclib and its derivatives are given in Table 2. Milciclib and its derivatives were predicted to be non-carcinogenic and have a class IIIacute oral toxicity according to AdmetSAR online database calculations. All the drugs exhibited a positive response towards the blood brain barrier, suggesting that milciclib and its derivatives are capable of passing through the blood-brain barrier. Moreover, all the drugs were also predicted to be P-glycoprotein (P-gp) inhibitors. P-gp is overexpressed on the surface of cancer cells, preventing medicines from being internalized and rendering chemotherapy ineffective [61]. Therefore, P-gp inhibition is required to increase the bioavailability of the drugs [62]. All drugs also exhibited a positive value for human intestinal absorption, suggesting that their bioavailability to be sufficiently high [63]. Moreover, Milciclib and its derivatives were found to be weak human Ether-à-go-go Related Gene (hERG) inhibitors. hERG inhibition can give rise to long QT syndrome, a lethal disorder linked with the risk of sudden cardiac death [64]. This aspect demands more research since all drugs seeking approval must be tested for their potential cardiac safety. Lipinski and coworkers' (1997) 'Rule of five' substantially aids in recognizing the drug likeliness and oral bioavailability of potentials drug candidates [65]. According to the Lipinski's rule, in order to avoid poor oral bioavailability, the molecular weight of a drug should be less than 500 Da, H-bond donors should be less than 5, H-bond acceptors should be less than 10 and octanol-water partition coefficient (log p) should not exceed 5 [66].Except for the D-CF_3 derivative, which had a molecular weight (Mwt) of 514, all of the medicines in our investigation had a Mwt of less than 500 Da. MedChem Designer software was utilized to obtain the Mwt, MlogP value, S + logP value, and S + logD value (Supplementary Table S3). Lipophilicity, which is the logarithm value of the partition coefficient P(logP) between

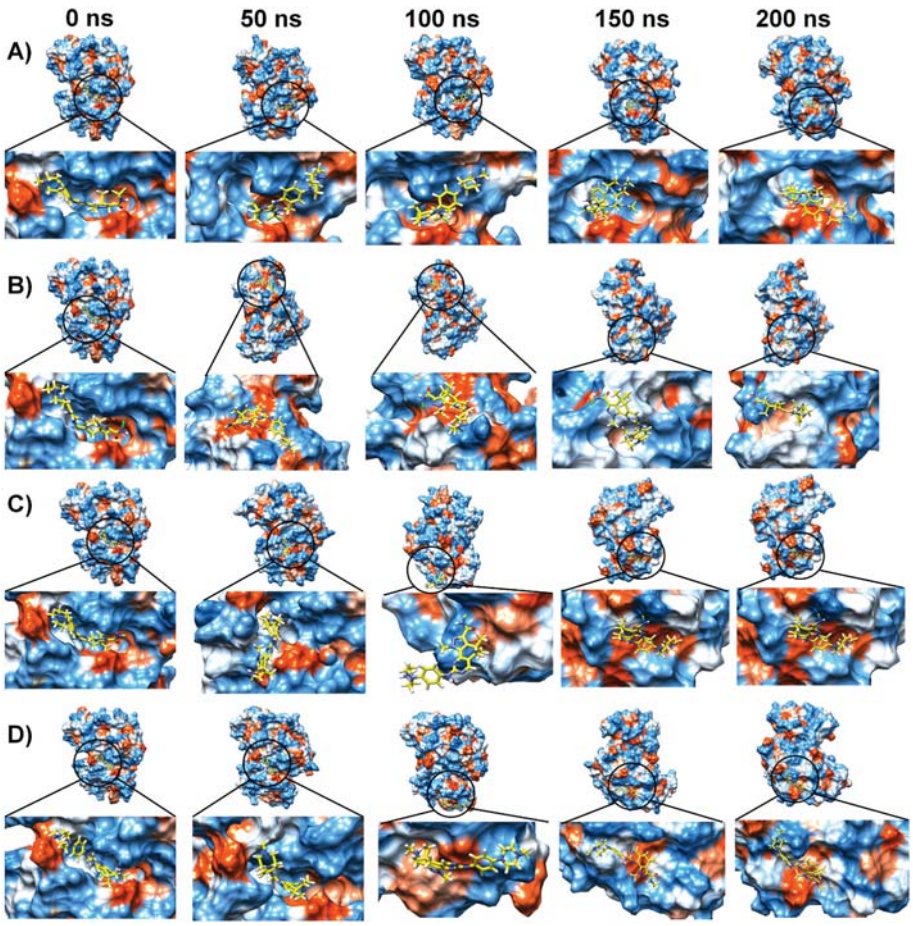

Fig. 5. The surface view snapshots taken at 0, 25, 50, 75 and 100 ns for A) D-CF_3-6Q4H complex, B) D-Cl-6Q4H complex, C) D-F-6Q4H complex, and B) D-milciclib-6Q4H complex (Surface representation according to hydrophobicity where blue represents hydrophilic, while orange represents hydrophobic surface. Ligand is shown in yellow stick representation). (For interpretation of the references to color in this figure legend, the reader is referred to the Web version of this article.)

octanol and water(buffer), performs as a crucial part in drug interaction with the receptor [67].All drugs in this study had a S + logP value of less than 5. This suggests that milciclib and its derivatives have a high permeability, as larger than 5 logP values indicate poor absorption or permeability of the drug [68]. MlogP (Moriguchi octanol-water partition coefficient), applied in QSAR model structure analysis, should be lower than 4.15 to penetrate biological membranes [69]. The MlogP value of all drugs in this study is significantly less than 4.15, advocating their ability to efficiently permeate biological membranes (Supplementary Table S3). To avoid poor oral bioavailability, the additional features outlined by Lipinski's, such as H-bond donors and bond acceptors, should be investigated for all medications.

All the drugs in this study exhibited toxicity less than 1.0 predicted by PreADMET are shown in Supplementary Table S4.

3.4. Molecular dynamics studies and MM-PBSA calculations

MDS offers a distinct advantage over rigid docking as it provides detailed insights into the binding of ligands at the binding site of the target protein [70]. It is particularly very useful in generating the trajectories of solvated and neutralized protein-ligand complex under simulated biological environment. In present study, we performed 200 ns MDS studies on four complexes of 6Q4H with ligands D-CF_3, D-Cl, D-F, and milciclib (D), respectively. The superimposed structures of pre- and post-MD states of both the complexes are shown in Fig. 4. There are no major secondary structural changes in the 6Q4H conformations.

The analysis of MD trajectories at various time intervals suggests that the ligand D-CF_3 and D-Cl remains bound at the binding pocket (Fig. 5) throughout the simulation period. The binding pocket, however, appears to adapt to the stable conformations of bound ligands. In the case of D-CF_3, the phenyl-piperidyl core moves out of the binding pocket. This may be due to the sterically bulky trifluoromethyl group which remains bound to the hydrophobic pocket throughout the simulation. The ligand D-Cl appears to be stable during initial 15 ns simulation, and at around 25 ns it moves out of the binding pocket. However, it occupies a slightly different binding pocket post 50 ns simulation period and remains stable until 200 ns. In the case of ligand D-F, the ligand remains stably bound till 50 ns simulation period. However, it occupies adjacent binding site after 75 ns till the end of simulation. On the other hand, milciclib remains bound in the binding pocket till 75 ns simulation period and during the last 25 ns simulation it moves out of this binding pocket and occupies slightly different surface binding pocket until the end of simulation period.

The conformational changes in the overall protein structure and ligand structure are estimated through protein backbone RMSD and RMSD in ligand atoms [71]. The lower the RMSD better is the conformational stability and the fewer the deviations from the initial positions of atoms. During the course of MDS, D-CF_3, D-Cl, D-F and milciclib complexes had average RMSD values of 0.267, 0.236, 0.240 and 0.245 nm for protein backbone atoms, respectively, indicating minor deviations in backbone atoms from initial positions (Table 3). These deviations are mostly originating from flexible loops. Moreover, these average RMSD values suggest that the complexes are reasonably stable, with the D-Cl complex being the most stable compared to other complexes (Fig. 6). All the complexes were found to be adequately stabilized after roughly 150 ns simulation. The D-Cl complex had substantial

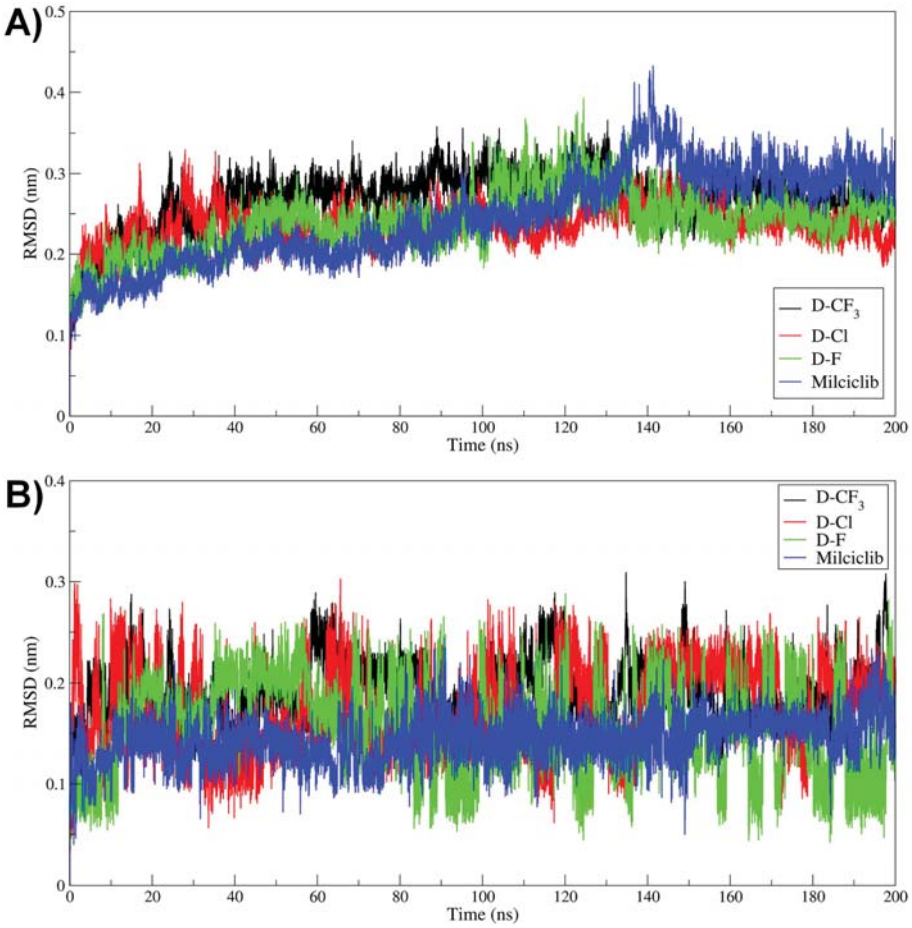

Fig. 6. RMSD for D-CF_3 D-Cl, D-F, and milciclib 6Q4H complexes. A) RMSD in protein backbone atoms, B) RMSD in ligand atoms.

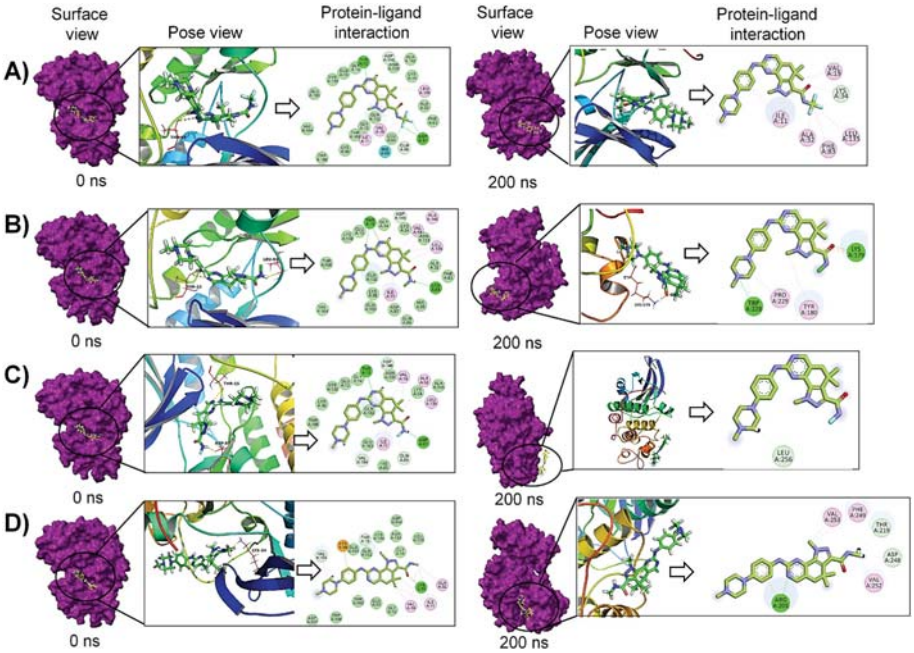

Fig. 7. Binding interactions captured from initial and last trajectory of MDS. A) D-CF_3 interactions, B) D-Cl interactions, C) D-F interactions, and B) D-milciclib interactions.

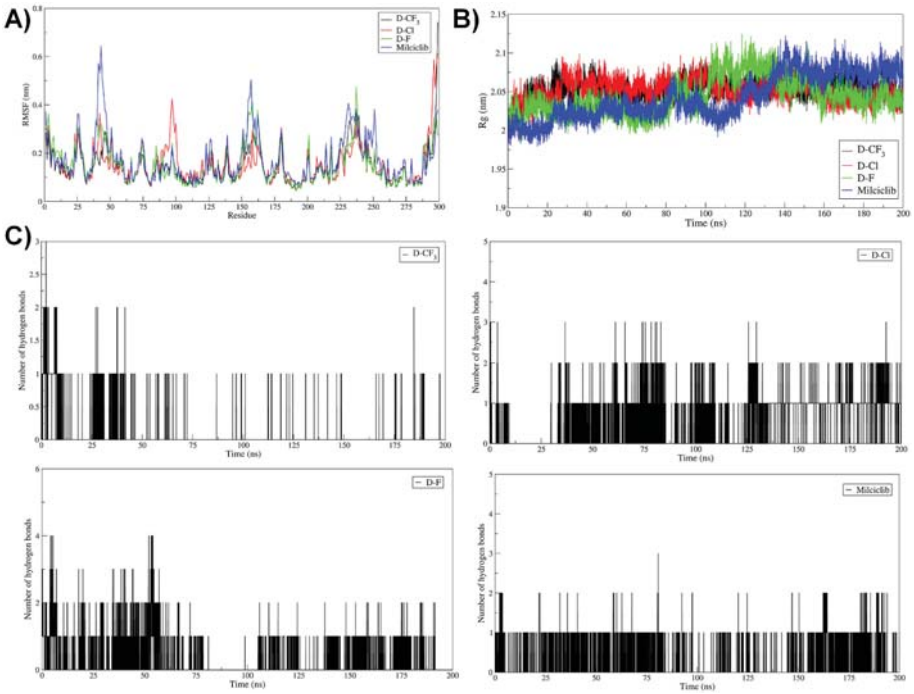

Fig. 8. (A)The results of RMSF measurement of the protein-ligand complexes, D-CF_3-6Q4H, D-Cl-6Q4H, D-F-6Q4H, and D-milciclib-6Q4H. (B) Radius of gyration (Rg) of Cα atoms of 6Q4H, and (C) The number of hydrogen bonds formed between the ligands, D-CF_3, D-Cl, D-F, and D-milciclib and binding site residues.

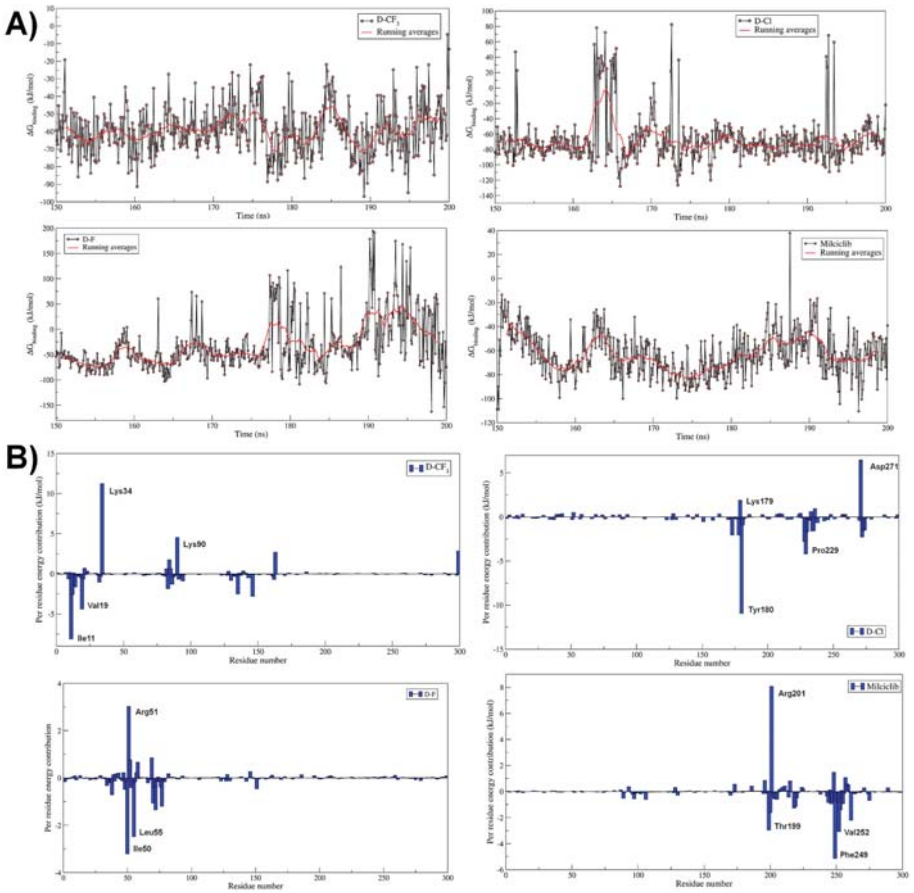

Fig. 9. MM-PBSA and domain decomposition analysis. A) Plots obtained from MM-PBSA calculations for binding energy versus MDS period, and B) Per residue energy contribution plots from domain decomposition studies.

Table 1
Binding affinity and non-bonding interaction of milciclib and derivatives D-F, D-Cl, and D-CF_3 with protein 6Q4H.

Compound	Binding energy (kcal/mol)	Hydrophobic bond (Distance Å)		Hydrogen Bond (Distance Å)	Halogen bond (Distance Å)	Electrostatic bond (Distance Å)
		Pi-alkyl	Alkyl			
D	−9.5	–	ILE10 (5.18) ILE10 (4.20) VAL18 (3.64) VAL163 (4.74)	LYS33 (2.86) LYS33 (2.67) THR14 (2.79) LYS33 (2.54)	–	LYS88 (4.63)
D-F	−10.3	VAL18 (5.48) ILE10 (5.20)	VAL18 (4.66) ALA31 (4.18) LEU134 (3.796) ALA144 (4.24)	THR14 (2.44) LEU83 (2.71) VAL163 (2.45)	–	ASP86 (4.51)
D-Cl	−10.2	ILE10 (5.45)	VAL18 (4.69) ALA31 (4.496) LEU134 (4.05) ALA144 (4.07) VAL18 (4.99)	THR14 (2.51) THR14 (2.15) ASP145 (2.66)	–	ASP86 (4.51)
D-CF_3	−10.3	ILE10 (5.35)	VAL18 (4.59) LEU134 (4.19) ALA144 (4.05) VAL18 (4.97)	THR14 (2.25) THR14 (2.21) ASP145 (2.51) GLN85 (2.42)	HIS84 (3.31) GLN85 (3.46) ASP86 (3.18)	ASP86 (4.76)

Table 2
AdmetSAR values of milciclib (D) and its derivatives (D-F, D-CF_3, D-Cl).

Parameters	D	D-F	D-CF_3	D-Cl
Blood brain barrier (BBB)	+ 0.7921	+ 0.7754	+ 0.7857	+ 0.7383
Human intestinal absorption	1.0000	1.0000	1.0000	1.0000
Caco-2 permeability	0.5915	0.6123	0.6453	0.5948
P-glycoprotein inhibitor	Inhibitor 0.8165	Inhibitor 0.7645	Inhibitor 0.8262	Inhibitor 0.6764
Human ether a-go-go-related (hERG) gene inhibition	0.8494	0.7645	0.9291	0.7667
Acute oral toxicity	III 0.6950	III 0.6325	III 0.6748	III 0.6281
Rat acute toxicity, LD_{50} (mol/kg)	2.7519	2.7794	2.7520	2.7691
Aqueous solubility	−3.2616	−3.4292	−3.6427	−3.5110
Carcinogen	NC (0.8010)	NC (0.7369)	NC (0.7540)	NC (0.7077)

Table 3
Average, minimum and maximum values of the MDS analysis.

Parameter	D-CF_3-CDK2 complex	D-Cl-CDK2 complex	D-F-CDK2 complex	Milciclib-CDK2 complex
Protein backbone atoms RMSD (nm)				
Average	0.267 (0.034)	0.236 (0.024)	0.240 (0.030)	0.245 (0.057)
Maximum	0.365	0.329	0.392	0.432
Minimum	0.076	0.076	0.071	0.065
Atoms of ligand RMSD (nm)				
Average	0.191 (0.029)	0.172 (0.041)	0.154 (0.045)	0.143 (0.022)
Maximum	0.308	0.302	0.287	0.244
Minimum	0.046	0.034	0.037	0.040
RMSF (nm)				
Average	0.148 (0.078)	0.157 (0.084)	0.154 (0.081)	0.173 (0.098)
Maximum	0.741	0.613	0.472	0.642
Minimum	0.045	0.050	0.046	0.061
Radius of Gyration (nm)				
Average	2.053 (0.012)	2.051 (0.013)	2.043 (0.022)	2.042 (0.029)
Maximum	2.093	2.098	2.124	2.121
Minimum	1.979	1.981	1.981	1.979

*Standard deviations in average values are given in parentheses.

deviations between 10 ns and 40 ns simulation before becoming stabilized.

The RMSD in ligand atoms clearly indicates that the conformation of D-Cl in the binding pocket is reasonably stable with considerably less deviations compared to the other ligands. The RMSD in D-CF_3 atoms is slightly higher than other ligands. However, D-CF_3 and D-Cl remains bound in the original binding pocket as evident from the visual inspection of the trajectories extracted at different time intervals. The average RMSD in ligand atoms for D-CF_3, D-Cl, D-F and milciclib are 0.191, 0.172, 0.154 and 0.143 nm respectively.

Table 4
Results of MM-PBSA calculations.

MM-PBSA energy component (kJ.mol^{-1})	D-CF_3	D-Cl	D-F	Milciclib
van der Waal energy	−121.683 (1.008)	−110.059 (0.695)	−68.859 (1.837)	−124.141 (0.962)
Electrostatic energy	−10.205 (0.215)	−15.923 (0.237)	−4.301 (0.254)	−3.649 (0.332)
Polar solvation energy	88.466 (1.115)	71.314 (1.483)	50.010 (2.344)	80.925 (1.053)
Solvent accessible surface area energy	−15.603 (0.120)	−13.181 (0.081)	−8.849 (0.223)	−16.306 (0.109)
Binding energy ($\Delta G_{binding}$)	−59.046 (0.606)	**−67.918** **(1.375)**	−32.092 (2.244)	−63.361 (0.844)

*Standard deviations are given in parentheses.

The stability of protein-ligand complex and overall elasticity of the residues of protein is evaluated in terms of RMSF measurement [72]. The larger fluctuations usually represent the diverse orientations and conformations of the side chain residues. The key residues involved in the hydrogen bond interactions include Ile10, Glu12, Thr14, Leu83, Lys33, Glu81, Phe82, His84, Gln85, Asp86, Lys129, and Gln131. These residues are likely to be the ones that show the most fluctuations during MDS. Fig. 7 shows the protein-ligand interactions captured from the initial poses and post-MD poses of the ligands, D-CF_3 D-Cl, D-F and milciclib, at the binding pocket of 6Q4H. The results of RMSF measurement are shown in Fig. 8A. According to the RMSF analysis, the residues ranging from 20 to 60, 75–110, and 150–175 show major fluctuations indicate that the binding site residues adapt to the ligand conformations as MDS progresses. The average RMSF of 0.148 and the maximum RMSF of 0.741 indicate that D-CF_3 binding favorably, generating fluctuations in the nearest region where it is undergoing conformational changes. The fluctuations in D-Cl complex reach a maximum RMSF of 0.613 with average RMSF of 0.157 which is slightly higher than D-CF_3 and D-F. The RMSF in D-F are minimal with an average RMSF of 0.154 with maximum RMSF of 0.472. Milciclib has highest RMSF with average RMSF of 0.173 nm indicating major fluctuations in the side chain atoms.

The analysis of Rg is another criterion to assess the root mean square

distance of a collection of atoms from their common center of mass and to provide an insight of the overall compactness of the system [73]. The Rg of milciclib complex is lowest with average of 2.042 nm. The D-F complex has the average Rg of 2.043 nm suggesting almost similar compactness of the system compared to milciclib complex. Other two complexes, D-CF_3 and C–Cl have slightly higher average Rg (Fig. 8B). The overall results of Rg suggest there are no major changes in the secondary structure of 6Q4H.

The ability of ligands to generate non-bonded interactions such as hydrogen bond interactions is thought to be due to their higher binding affinity [74]. One of the parameters used to assess the binding affinity and stability of a protein-ligand complex is the number of hydrogen bonds formed and the lifetime of these hydrogen bonds. One hydrogen bond was seen consistently being formed during initial 80 ns and post 150 ns MDS period in the case of milciclib complex (Fig. 8C). The maximum number of hydrogen bonds formed for this complex in any one timeframe is 3. On the other hand, around 2 hydrogen bonds were found consistently formed during initial 50 ns simulation and one hydrogen bond thereafter until the end of simulation period for D-F complex with maximum number of hydrogen bonds formed 4. Fig. 8C shows that two hydrogen bonds were consistently formed with D-Cl complex after around 30 ns of MDS until the end of simulation period. In the case of D-CF_3 complex only one hydrogen bond was seen formed intermittently throughout the simulation. The hydrogen bond occupancy analysis suggests that the nitrogen atom of D-CF_3 forms a hydrogen bond with His85 with prominent occupancy of 5.9%. Similarly, the same nitrogen atom from pyrazole ring in D-F was found forming a hydrogen bond with Glu13 with the occupancy of 7.2%. (Supplementary Fig. S4). Interestingly, the hydrogen atom from –CONHCl group in D-Cl forms a hydrogen bond with His72 residue with occupancy of 12.4% and nitrogen atom from piperazine ring forms hydrogen bond with residue Trp228 with highest occupancy of 35.9%. This donor-acceptor hydrogen bond was not formed in the case of milciclib probably due to the serically bulkier –CH_3 group and due to other hydrogen bonds with acceptor nitrogen atoms in milciclib. In the case of milciclib the oxygen atom from –$CONHCH_3$ group forms prominent hydrogen bond with Lys34 residue with occupancy 5.6%. These findings suggest that D-Cl makes more favorable non-bonded interactions such as hydrogen bond interactions at the binding pocket and thus may have better binding affinity than other derivatives, D-CF_3 and D-F.

In order to evaluate the binding affinity, the MM-PBSA calculations were performed on both the systems. In terms of binding free energy, the MM-PBSA calculations provides more accurate estimates of binding affinity [44]. In the MM-PBSA calculations, van der Waal energy, electrostatic energy, polar solvation energy, SASA energy and binding energy are evaluated by solving equations of continuum electrostatics of bio-molecular systems under study by APBS (Adaptive Poisson-Boltzmann Solver) method [75]. During the estimation of the binding free energy ($\Delta G_{binding}$), non-bonded interactions such as van der Waal energy and electrostatic energy measured in terms of Coulomb and Lennard-Jones (LJ) potential functions respectively is taken into the account. The trajectories originating from 150 till 200 ns isolated at each 100 ps were employed in the MM-PBSA calculations. The results showed that D-Cl has the lower binding energy (−67.918 kJ.mol-1) amongst all the studied complexes (Table 4). The derivative D-CF_3 has comparable binding energy (−59.046 kJ.mol^{-1}) to milciclib (−63.361 kJ.mol^{-1}). The derivative D-F has slightly unfavorable binding energy (−32.092 kJ.mol^{-1}) compared to other ligands. The van der Waal energy and polar salvation energy influence the binding energy in D-Cl and milciclib favorably. It is evident that replacing –Cl having slightly lower polar salvation energy with electronegative –CF_3 results in significant increase in polar salvation energy and consequently the derivative D-CF_3 has slightly higher binding energy compared to D-Cl derivative. Slightly higher van der Waal energy and least polar solvation energy results in higher binding energy in the case of D-F derivative. The binding energies of each isolated trajectories for these complexes are shown in Fig. 9A. The per residue domain decomposition studies were also performed to understand the key contribution of the residues in these binding energies Fig. 9B. In case of D-CF_3, the residue Ile11 and Val19 were found prominently contributing in binding energy. While, the residue Lys34 and Lys90 have positive energy contribution (above +5 kJ.mol^{-1}) in this derivative. In the case of derivative D-Cl, the residue Tyr180 and Pro229 has favorable energy contributions in terms of binding energy, while basic and acidic residues Lys179 and Asp27 respectively have favorable contributions in terms of electrostatic energy. The residues Ile50 and Leu55 have favorable energies in the case of D-F derivative, while Arg51 has unfavorable energy contribution in the binding energy of D-F derivate. Per residue decomposition analysis in milciclib showed that the residues Thr199, Phe249, and Val252 have favorable energies, while the residue Arg201 contributes unfavorably. In the case of D-Cl the favorably contributing residues have energy contributions better than −5 kJ.mol^{-1} compared to other ligands.

4. Conclusion

Our study demonstrated the binding interactions of halogenated milciclib ligands with crystal structures of CDK2. We have employed a series of halogen-directed milciclib drugs and subjected them to molecular orbital calculations, molecular docking, non-bonded interaction analysis, pharmacokinetic analysis, MDS and MM-PBSA calculations. Our analyses suggest that halogenation has improved the binding energy, binding affinity and pharmacokinetic properties of the parent drug milciclib. There were some inconsistencies as the HOMO-LUMO energy gap of the parent drug was found to be reasonably lower than its derivatives, indicating that the parent drug was more chemically reactive. Our findings, however, confirmed that –CF_3 and –Cl directed modifications resulted in significant chemical reactivity, the best binding affinity, excellent nonbonding interactions, and better pharmacokinetic properties compared to the parent drug. Among the best ligands, D-Cl and D-CF_3 had a slightly more stable conformation and higher binding affinity compared to D-F as evaluated by MDS and MM-PBSA calculations. Halogenation of milciclib holds promising therapeutic potential as HCC therapy. However, further *in vitro* and *in vivo* studies are required to validate the anticancer efficacy of these ligands.

Ethics approval and consent to participate

Not Applicable.

Consent for publication

Not Applicable.

Availability of data and material

All the data generated during the experiment are provided in the manuscript/supplementary material.

Funding

No funding was received from any external sources.

Declaration of competing interest

The authors declare that they have no known competing financial interests or personal relationships that could have appeared to influence the work reported in this paper.

Acknowledgements

Authors are thankful to the Department of Pharmaceutical Chemistry, Sinhgad College of Pharmacy, Maharashtra, India, and the

Department of Pharmacy, Bangabandhu Sheikh Mujibur Rahman Science and Technology University, Bangladesh for providing support to successfully carry out the research.

Appendix A. Supplementary data

Supplementary data to this article can be found online at https://doi.org/10.1016/j.imu.2022.101069.

References

[1] Kim E, Viatour P. Hepatocellular carcinoma: old friends and new tricks. Exp Mol Med 2020;52(12):1898–907. https://doi.org/10.1038/s12276-020-00527-1.

[2] Ghouri YA, Mian I, Rowe JH. Review of hepatocellular carcinoma: epidemiology, etiology, and carcinogenesis. J Carcinog 2017. https://doi.org/10.4103/jcar.JCar_9_16.

[3] Raza A, Sood GK. Hepatocellular carcinoma review: current treatment, and evidence-based medicine. World J Gastroenterol 2014;20(15):4115. https://doi.org/10.3748/wjg.v20.i15.4115.

[4] Shen S, Dean DC, Yu Z, Duan Z. Role of cyclin-dependent kinases (CDKs) in hepatocellular carcinoma: therapeutic potential of targeting the CDK signaling pathway. Hepatol Res 2019;49(10):1097–108. https://doi.org/10.1111/hepr.13353.

[5] Harper JV, Brooks G. The mammalian cell cycle. In: Humphrey T, Brooks G, editors. Cell cycle control: mechanisms and protocols. Totowa, NJ: Humana Press; 2005. p. 113–53. https://doi.org/10.1385/1-59259-857-9:113.

[6] Oudah KH, Abdou NS, Serya RAT, Abouzid KAM. An overview on the prospective CDKs inhibitors as anti-cancer drugs: review article. J. Am. Sci. 2017;13(4):6–23. https://doi.org/10.7537/marsjas130417.02.

[7] Bonelli P, Tuccillo FM, Borrelli A, Schiattarella A, Buonaguro FM. CDK/CCN and CDKI alterations for cancer prognosis and therapeutic predictivity. BioMed. Res. Int, Jan. 2014. https://doi.org/10.1155/2014/361020.

[8] Borgne A, Versteege I, Mahé M, Studeny A, Léonce S, Naime I, et al. Analysis of cyclin B1 and CDK activity during apoptosis induced by camptothecin treatment. Oncogene 2006;25:7361–72. https://doi.org/10.1038/sj.onc.1209718.

[9] Hou Y, Wang Z, Huang S, Sun C, Zhao J, Shi J, et al. SKA3 Promotes tumor growth by regulating CDK2/P53 phosphorylation in hepatocellular carcinoma. Cell Death Dis 2019;10:1–15. https://doi.org/10.1038/s41419-019-2163-3.

[10] Jindal A, Thadi A, Shailubhai K. Hepatocellular carcinoma: etiology and current and future drugs. J. Clin. Exp. Hepatol. 2019;9(2):221–32. https://doi.org/10.1016/j.jceh.2019.01.004.

[11] B. Douglas Guy Cheung, C. M. Croce, A. Kay Huebner, and D. Guttridge, Action of CDK inhibitor PHA-848125 in ER-negative breast cancer with MicroRNA-221/222 overexpression.

[12] Brasca MG, Amboldi N, Ballinari D, Cameron A, Casale E, Cervi G, et al. Identification of N,1,4,4-tetramethyl-8-{[4-(4-methylpiperazin-1-yl) phenyl] amino}-4,5-dihydro-1H-pyrazolo [4,3-h] quinazoline-3-carboxamide (PHA-848125), a potent, orally available cyclin dependent kinase inhibitor. J Med Chem 2009;52:5152–63.

[13] Martínez-Chávez A, Tibben MM, Broeders J, Rosing H, Schinkel AH, Beijnen JH. Development and validation of an LC-MS/MS method for the quantitative analysis of milciclib in human and mouse plasma, mouse tissue homogenates and tissue culture medium. J Pharm Biomed Anal Oct 2020;190:113516. https://doi.org/10.1016/j.jpba.2020.113516.

[14] Parisini E, Metrangolo P, Pilati T, Resnati G, Terraneo G. Halogen bonding in halocarbon–protein complexes: a structural survey. Chem Soc Rev 2011;40(5):2267–2278, Apr. https://doi.org/10.1039/c0cs00177e.

[15] Hardegger LA, et al. Systematic investigation of halogen bonding in protein-ligand interactions. Angew Chem Int Ed Jan. 2011;50(1):314–8. https://doi.org/10.1002/anie.201006781.

[16] Auffinger P, Hays FA, Westhof E, Ho PS. Halogen bonds in biological molecules. Proc. Natl. Acad. Sci. U.S.A Nov. 2004;101(48):16789–94. https://doi.org/10.1073/pnas.0407607101.

[17] Uddin N, Ahmed S, Khan AM, Mazharol Hoque M, Halim MA. Halogenated derivatives of methotrexate as human dihydrofolate reductase inhibitors in cancer chemotherapy. J Biomol Struct Dyn Feb. 2020;38(3):901–17. https://doi.org/10.1080/07391102.2019.1591302.

[18] Voth AR, Hays FA, Ho PS. Directing macromolecular conformation through halogen bonds. Proc. Natl. Acad. Sci. U.S.A 2007;104(15):6188–6193, Apr. https://doi.org/10.1073/pnas.0610531104.

[19] Kolár M, Hobzaa P, Bronowska AK. Plugging the explicit σ-holes in molecular docking. Chem Commun Jan. 2013;49(10):981–3. https://doi.org/10.1039/c2cc37584b.

[20] Alonso C, Martínez De Marigorta E, Rubiales G, Palacios F. Carbon trifluoromethylation reactions of hydrocarbon derivatives and heteroarenes. Chem Rev Feb. 25, 2015;115(4):1847–935. https://doi.org/10.1021/cr500368h. American Chemical Society.

[21] Champagne PA, Desroches J, Hamel JD, Vandamme M, Paquin JF. Monofluorination of organic compounds: 10 Years of innovation. Chem Rev 2015;115(17):9073–174. https://doi.org/10.1021/cr500706a. American Chemical Society.

[22] Hagmann WK. The many roles for fluorine in medicinal chemistry. J Med Chem 2008. https://doi.org/10.1021/jm800219f.

[23] Purser S, Moore PR, Swallow S, Gouverneur V. Fluorine in medicinal chemistry. Chem Soc Rev 2008. https://doi.org/10.1039/b610213c.

[24] Li Q, Cheng T, Wang Y, Bryant SH. PubChem as a public resource for drug discovery. Drug Discov Today 2010. https://doi.org/10.1016/j.drudis.2010.10.003.

[25] Schneider HJ, Hacket F, Rüdiger V, Ikeda H. NMR studies of cyclodextrins and cyclodextrin complexes. Chem Rev 1998. https://doi.org/10.1021/cr970019t.

[26] Sompornpisut P, Deechalao N, Vongsvivut J. An inclusion complex of -Cyclodextrin-L-Phenylalanine: 1H NMR and molecular docking studies. Sci Asia 2002. https://doi.org/10.2306/scienceasia1513-1874.2002.28.263.

[27] Rose PW, et al. The RCSB protein Data Bank: new resources for research and education. Nucleic Acids Res 2013. https://doi.org/10.1093/nar/gks1200.

[28] DeLano WL. Pymol: an open-source molecular graphics tool. CCP4 Newsl. Protein Crystallogr.; 2002.

[29] Morris GM, Lim-Wilby M. Molecular docking. Methods Mol Biol 2008. https://doi.org/10.1007/978-1-59745-177-2_19.

[30] Trott O, Olson AJ. Autodock vina: improving the speed and accuracy of docking with a new scoring function, efficient optimization and multithreading. J Comput Chem 2010. https://doi.org/10.1002/jcc.

[31] Cheng F, Li W, Zhou Y, Shen J. admetSAR: a comprehensive source and free tool for evaluating chemical ADMET properties. J Chem Inf Model 2012. https://doi.org/10.1021/ci300367a.

[32] Roman DL, Roman M, Som C, Schmutz M, Hernandez E, Wick P, Casalini T, Perale G, Ostafe V, Isvoran A. Computational assessment of the pharmacological profiles of degradation products of chitosan. Front Bioeng Biotechnol Sep 2019;6(7):214. https://doi.org/10.3389/fbioe.2019.00214.

[33] Berendsen HJC, van der Spoel D, van Drunen R. GROMACS: a message-passing parallel molecular dynamics implementation. Comput Phys Commun 1995 Sep;91(1–3):43–56. https://doi.org/10.1016/0010-4655(95)00042-E.

[34] S A, Tl B. Comparative protein modelling by satisfaction of spatial restraints [Internet]. J Mol Biol 1993. https://doi.org/10.1006/jmbi.1993.1626 [cited 2020 Jul 18].

[35] Best RB, Zhu X, Shim J, Lopes PEM, Mittal J, Feig M, et al. Optimization of the additive CHARMM all-atom protein force field targeting improved sampling of the backbone φ, ψ and side-chain χ1 and χ2 dihedral angles. J Chem Theor Comput 2012 Sep 11;8(9):3257–73. https://doi.org/10.1021/ct300400x.

[36] Vanommeslaeghe K, Hatcher E, Acharya C, Kundu S, Zhong S, Shim J, et al. CHARMM general force field: a force field for drug-like molecules compatible with the CHARMM all-atom additive biological force fields. J Comput Chem 2009. https://doi.org/10.1002/jcc.21367. NA-NA.

[37] Yu W, He X, Vanommeslaeghe K, MacKerell AD. Extension of the CHARMM general force field to sulfonyl-containing compounds and its utility in biomolecular simulations. J Comput Chem 2012 Dec 5;33(31):2451–68. https://doi.org/10.1002/jcc.23067.

[38] Berendsen HJC, Postma JPM, van Gunsteren WF, Hermans J. Interaction models for water in relation to protein hydration. In: Pullman B, editor. Intermolecular forces [internet]. Dordrecht: Springer Netherlands; 1981. p. 331–42. https://doi.org/10.1007/978-94-015-7658-1_21 [cited 2021 Jun 19].

[39] Bussi G, Donadio D, Parrinello M. Canonical sampling through velocity rescaling. J Chem Phys 2007 Jan 7;126(1):014101. https://doi.org/10.1063/1.2408420.

[40] Berendsen HJC, Postma JPM, van Gunsteren WF, DiNola A, Haak JR. Molecular dynamics with coupling to an external bath. J Chem Phys 1984 Oct 15;81(8):3684–90. https://doi.org/10.1063/1.448118.

[41] Hess B, Bekker H, Berendsen HJC, Fraaije JGEM. LINCS: a linear constraint solver for molecular simulations. J Comput Chem 1997 Sep;18(12):1463–72. https://doi.org/10.1021/ct700200b.

[42] Petersen HG. Accuracy and efficiency of the particle mesh Ewald method. J Chem Phys 1995 Sep;103(9):3668–79. https://doi.org/10.1063/1.470043.

[43] Parrinello M, Rahman A. Polymorphic transitions in single crystals: a new molecular dynamics method. J Appl Phys 1981 Dec;52(12):7182–90. https://doi.org/10.1063/1.328693.

[44] Kumari R, Kumar R. Open-source drug discovery consortium, lynn A. g_mmpbsa - a GROMACS tool for high-throughput MM-PBSA calculations. J Chem Inf Model 2014 Jul 28;54(7):1951–62. https://doi.org/10.1021/ci500020m.

[45] Baker NA, Sept D, Joseph S, Holst MJ, McCammon JA. Electrostatics of nanosystems: application to microtubules and the ribosome. Proc Natl Acad Sci USA 2001 Aug 28;98(18):10037–41. https://doi.org/10.1073/pnas.181342398.

[46] Fukui K, Yonezawa T, Shingu H. A molecular orbital theory of reactivity in aromatic hydrocarbons. J Chem Phys 1952. https://doi.org/10.1063/1.1700523.

[47] Parr RG, Zhou Z. Absolute hardness: unifying concept for identifying shells and subshells in nuclei, atoms, molecules, and metallic clusters. Acc Chem Res 1993. https://doi.org/10.1021/ar00029a005.

[48] Hoque MM, Halim MA, Sarwar MG, Khan MW. Palladium-catalyzed cyclization of 2-alkynyl-N-ethanoyl anilines to indoles: synthesis, structural, spectroscopic, and mechanistic study. J Phys Org Chem 2015. https://doi.org/10.1002/poc.3477.

[49] Pearson WR, Lipman DJ. Improved tools for biological sequence comparison. Proc. Natl. Acad. Sci. U.S.A 1988. https://doi.org/10.1073/pnas.85.8.2444.

[50] Li J, Fu A, Zhang L. An overview of scoring functions used for protein–ligand interactions in molecular docking. Interdiscipl Sci Comput Life Sci 2019. https://doi.org/10.1007/s12539-019-00327-w.

[51] Lishchynskyi A, Novikov MA, Martin E, Escudero-Adán EC, Novák P, Grushin VV. Trifluoromethylation of aryl and heteroaryl halides with fluoroform-derived CuCF3: scope, limitations, and mechanistic features. J Org Chem 2013. https://doi.org/10.1021/jo401423h.

[52] Gillis EP, Eastman KJ, Hill MD, Donnelly DJ, Meanwell NA. Applications of fluorine in medicinal chemistry. J Med Chem 2015. https://doi.org/10.1021/acs.jmedchem.5b00258.
[53] Bissantz C, Kuhn B, Stahl M. Erratum: a medicinal chemistguide to molecular interactions (Journal of Medicinal Chemistry (2010) 53 (5061) DOI: 10.1021/jm100112j) J Med Chem 2010. https://doi.org/10.1021/jm100950p.
[54] Hunter CA. Quantifying intermolecular interactions: guidelines for the molecular recognition toolbox. Angew Chem Int Ed 2004. https://doi.org/10.1002/anie.200301739.
[55] Wade RC, Goodford PJ. The role of hydrogen-bonds in drug binding. Prog Clin Biol Res 1989;289:433–44.
[56] Shawon J, et al. Molecular recognition of azelaic acid and related molecules with DNA polymerase I investigated by molecular modeling calculations. Interdiscipl Sci Comput Life Sci Sep. 2018;10(3):525–37. https://doi.org/10.1007/s12539-016-0186-3.
[57] Zhao GJ, Liu JY, Zhou LC, Han KL. Site-selective photoinduced electron transfer from alcoholic solvents to the chromophore facilitated by hydrogen bonding: a new fluorescence quenching mechanism. J Phys Chem B Aug. 2007;111(30):8940–5. https://doi.org/10.1021/jp0734530.
[58] Zhao G-J, Han K-L. Site-specific solvation of the photoexcited protochlorophyllide a in methanol: formation of the hydrogen-bonded intermediate state induced by hydrogen-bond strengthening. Biophys J 2008;94:38–46. https://doi.org/10.1529/biophysj.107.113738.
[59] Lu Y, Liu Y, Xu Z, Li H, Liu H, Zhu W. Halogen bonding for rational drug design and new drug discovery. Expet Opin Drug Discov 2012. https://doi.org/10.1517/17460441.2012.678829.
[60] Egli M, Tereshko V, Mushudov GN, Sanishvili R, Liu X, Lewis FD. Face-to-face and edge-to-face π-π interactions in a synthetic DNA hairpin with a stilbenediether linker. J Am Chem Soc 2003. https://doi.org/10.1021/ja0355527.
[61] Amin ML. P-glycoprotein inhibition for optimal drug delivery. Drug Target Insights 2013. https://doi.org/10.4137/DTI.S12519.
[62] Kruijtzer CMF, et al. Increased oral bioavailability of topotecan in combination with the breast cancer resistance protein and P-glycoprotein inhibitor GF120918. J Clin Oncol 2002. https://doi.org/10.1200/JCO.2002.12.116.
[63] Shen J, Cheng F, Xu Y, Li W, Tang Y. Estimation of ADME properties with substructure pattern recognition. J Chem Inf Model 2010. https://doi.org/10.1021/ci100104j.
[64] Witchel HJ. Drug-induced hERG block and long QT syndrome. Cardiovascular Therapeutics 2011;29:251–9. https://doi.org/10.1111/j.1755-5922.2010.00154.x.
[65] Fernandes TB, Segretti MCF, Polli MC, Parise-Filho R. Analysis of the applicability and use of Lipinski's rule for central nervous system drugs. Lett Drug Des Discov 2016. https://doi.org/10.2174/1570180813666160622092839.
[66] Lipinski CA, Lombardo F, Dominy BW, Feeney PJ. Experimental and computational approaches to estimate solubility and permeability in drug discovery and development settings. Adv Drug Deliv Rev 1997. https://doi.org/10.1016/S0169-409X(96)00423-1.
[67] McKim J, Schmieder P, Veith G. Absorption dynamics of organic chemical transport across trout gills as related to octanol-water partition coefficient. Toxicol Appl Pharmacol 1985. https://doi.org/10.1016/0041-008X(85)90262-5.
[68] Rout S, Mahapatra RK. In silico screening of novel inhibitors of M17 Leucine Amino Peptidase (LAP) of Plasmodium vivax as therapeutic candidate. Biomed Pharmacother Aug. 2016;82:192–201. https://doi.org/10.1016/j.biopha.2016.04.057.
[69] Cheng T, et al. Computation of octanol-water partition coefficients by guiding an additive model with knowledge. J Chem Inf Model 2007. https://doi.org/10.1021/ci700257y.
[70] Salo-Ahen OMH, Alanko I, Bhadane R, Bonvin AMJJ, Honorato RV, Hossain S, et al. Molecular dynamics simulations in drug discovery and pharmaceutical development. Processes 2020 Dec 30;9(1):71. https://doi.org/10.3390/pr9010071.
[71] Sargsyan K, Grauffel C, Lim C. How molecular size impacts RMSD applications in molecular dynamics simulations. J Chem Theor Comput 2017 Apr 11;13(4):1518–24. https://doi.org/10.1021/acs.jctc.7b00028.
[72] Martínez L. Automatic identification of mobile and rigid substructures in molecular dynamics simulations and fractional structural fluctuation analysisKleinjung J, editor. PLoS One 2015 Mar 27;10(3):e0119264. https://doi.org/10.1371/journal.pone.0119264.
[73] MYu Lobanov, Bogatyreva NS, Galzitskaya OV. Radius of gyration as an indicator of protein structure compactness. Mol Biol 2008 Aug;42(4):623–8.
[74] Eastman P, Pande VS. Efficient nonbonded interactions for molecular dynamics on a graphics processing unit. J Comput Chem 2009. https://doi.org/10.1002/jcc.21413. NA-NA.
[75] Jurrus E, Engel D, Star K, Monson K, Brandi J, Felberg LE, et al. Improvements to the APBS biomolecular solvation software suite. Protein Sci 2018 Jan;27(1):112–28. https://doi.org/10.1002/pro.3280.